AMERICAN SOCIETY FOR MICROBIOLOGY | Infection and Immunity®

HOST RESPONSE AND INFLAMMATION

Depletion of Alveolar Macrophages Increases Pulmonary Neutrophil Infiltration, Tissue Damage, and Sepsis in a Murine Model of *Acinetobacter baumannii* Pneumonia

Hiu Ham Lee,[a,b] Lilit Aslanyan,[a] Arjun Vidyasagar,[a] Melissa B. Brennan,[b] Maxine S. Tauber,[b] Maria A. Carrillo-Sepulveda,[a] Michael R. Dores,[c] Nathan W. Rigel,[c] Luis R. Martinez[a,b,d]

[a]Department of Biomedical Sciences, NYIT College of Osteopathic Medicine, New York Institute of Technology, Old Westbury, New York, USA
[b]Department of Biomedical Sciences, Long Island University-Post, Brookville, New York, USA
[c]Department of Biology, Hofstra University, Hempstead, New York, USA
[d]Department of Oral Biology, University of Florida College of Dentistry, Gainesville, Florida, USA

Hiu Ham Lee and Lilit Aslanyan contributed equally and share first authorship. Author order was determined on the basis of initial involvement in the project.

ABSTRACT *Acinetobacter baumannii* has emerged as an important etiological agent of hospital-related infections, especially nosocomial pneumonia. The virulence factors of this bacterium and their interactions with the cells and molecules of the immune system just recently began to be extensively studied. Here, we investigated the impact of alveolar macrophages on *A. baumannii* pneumonia using a mouse model of infection and a flexible tissue culture system. We hypothesized that depletion of macrophages would enhance sepsis and severity of *A. baumannii* disease. We showed that macrophages are important for modulating the antibacterial function of neutrophils and play an important role in eradicating *A. baumannii* infection *in vivo*. Our findings suggest that in the absence of macrophages in the lungs, *A. baumannii* replicates significantly, and host proinflammatory cytokines are considerably reduced. Neutrophils are abundantly recruited to pulmonary tissue, releasing high amounts of reactive oxygen species and causing extensive tissue damage. The ability of *A. baumannii* to form biofilms and resist oxidative stress in the respiratory tract facilitates systemic dissemination and ultimately death of infected C57BL/6 mice. These results provide novel information regarding *A. baumannii* pathogenesis and may be important for the development of therapies aimed at reducing morbidity and mortality associated with this emerging bacterial pathogen.

KEYWORDS *A. baumannii*, apoptosis, cytokines, inflammation, macrophages, neutrophils

The Gram-negative bacterium *Acinetobacter baumannii* has become an increasingly prevalent cause of hospital-acquired pneumonic infections in immunocompromised patients (1). This microbe became notorious by causing disease among U.S. military personnel deployed in Iraq and Afghanistan (2). The majority of clinical isolates display high resistance to commonly used antimicrobial drugs, further complicating successful medical interventions (1, 3). Interestingly, *A. baumannii* also exhibits multiple virulence factors, which allow for host colonization via multiple routes of transmission (4), resistance to desiccation (5, 6), the capacity to form biofilms (7, 8), the ability to regulate iron intake (9, 10), and a proclivity for acquiring antibiotic resistance (11). Immunocompromised patients are at particular risk for *A. baumannii* infection via aerosol droplets, skin-to-skin contact, or exposure to contaminated medical equipment (4). In severe cases, *A. baumannii* can disseminate to the bloodstream resulting in

Citation Lee HH, Aslanyan L, Vidyasagar A, Brennan MB, Tauber MS, Carrillo-Sepulveda MA, Dores MR, Rigel NW, Martinez LR. 2020. Depletion of alveolar macrophages increases pulmonary neutrophil infiltration, tissue damage, and sepsis in a murine model of *Acinetobacter baumannii* pneumonia. Infect Immun 88:e00128-20. https://doi.org/10.1128/IAI.00128-20.

Editor Victor J. Torres, New York University School of Medicine

Address correspondence to Luis R. Martinez, lmartinez@dental.ufl.edu.

Received 4 March 2020
Returned for modification 5 April 2020
Accepted 30 April 2020
Accepted manuscript posted online 4 May 2020
Published 22 June 2020

septicemia. Despite its growing clinical importance, little is known about the cellular and molecular mechanisms behind the host defenses against *A. baumannii* infections.

Innate or natural immunity plays a crucial role in determining the outcome of bacterial pulmonary infections. For instance, strains of *A. baumannii* resistant to early innate effectors are able to establish very high bacterial cell density in the bloodstream, and subsequent sustained bacteremia leads to Toll-like receptor 4 (TLR-4)-mediated hyperinflammation and lethality (12). Also, depletion of neutrophils with antibodies to Ly-6G (13) and Gr-1 (14) has shown that *A. baumannii* establishes infections in murine models of pneumonia and skin infections (15). Similarly, macrophages demonstrate an important role in the early immune response to acute *A. baumannii* infections by eliminating microbes through phagocytic mechanisms as well as the production of inflammatory cytokines (16). In contrast, macrophages are also important anti-inflammatory cells that release cytokines that reduce the harmful effects of collateral tissue damage due to infection or excessive neutrophil infiltration (17).

This study aimed to explore and understand the role of alveolar macrophages during *A. baumannii* pulmonary infection. Clodronate in liposomes specifically induces apoptosis of macrophages and was used to deplete these phagocytic cells prior to bacterial infection. Hence, we hypothesized that a reduction in the number of alveolar macrophages would facilitate sepsis and increase severity of *A. baumannii* disease in an experimental murine model of pneumonia. Similar to other studies (12, 16), our findings indicate that macrophages play an essential and regulatory role in the early eradication of *A. baumannii* in the setting of pneumonia. However, our study specifically demonstrated that macrophages modulate the host cellular and molecular responses while containing the bacteria in the respiratory system. These results are important because they expand our knowledge of *A. baumannii* pathogenesis and may lead to the development of specific therapeutic strategies limiting the dissemination of the bacterium, therefore reducing *A. baumannii* morbidity and mortality.

RESULTS

Clodronate-treated mice show reduced survival in *A. baumannii* infection. To assess the interplay of immune effector cells in response to infection with *A. baumannii*, we employed a liposome-delivered system to selectively deplete macrophages. Upon reducing the pool of available macrophages, we observed an acceleration in mortality of *A. baumannii*-infected mice compared to that of control mice ($P < 0.01$) (Fig. 1). Seventy-two hours postinfection, 100% of clodronate-treated mice had died in comparison to 20% of the untreated mice. On average, clodronate-treated mice died of *A. baumannii*-mediated pneumonia 48 h postinfection compared to 108 h postinfection for untreated mice (Fig. 1A). In mice challenged with a sublethal dose of *A. baumannii*, the pulmonary bacterial burden of clodronate-treated animals was significantly higher than that of untreated mice early after infection (4 h, $P < 0.001$; 24 h, $P < 0.0001$; and 48 h, $P < 0.00001$) (Fig. 1B). Macrophage-depleted mice showed a 3 log increase in bacterial load in the lungs relative to that of control animals 48 h postinfection ($P < 0.00001$).

Histological examination revealed that untreated and clodronate-treated *A. baumannii*-infected mice had substantial inflammation by 48 h postinfection (Fig. 1C). Likewise, clodronate-treated and infected mice displayed considerably localized peribronchial inflammation with excessive infiltration of inflammatory cells within the alveoli (Fig. 1C) and a higher lung injury score (LIS; $P < 0.001$) (Fig. 1D) than the untreated controls. Gram staining showed presence of Gram-negative bacteria within the alveolar spaces of the lungs of infected control and clodronate-treated mice (Fig. 1C; insets). Additionally, clodronate-treated mice showed a significantly higher (2 to 3 log) microbial load in circulation 24 h postinfection than that of untreated mice and maintained this burden 48 h postinfection ($P < 0.00001$) (Fig. 1E). These findings demonstrated that macrophage depletion enhances *A. baumannii* pathogenesis by increasing pulmonary load and presence of bacteria in blood.

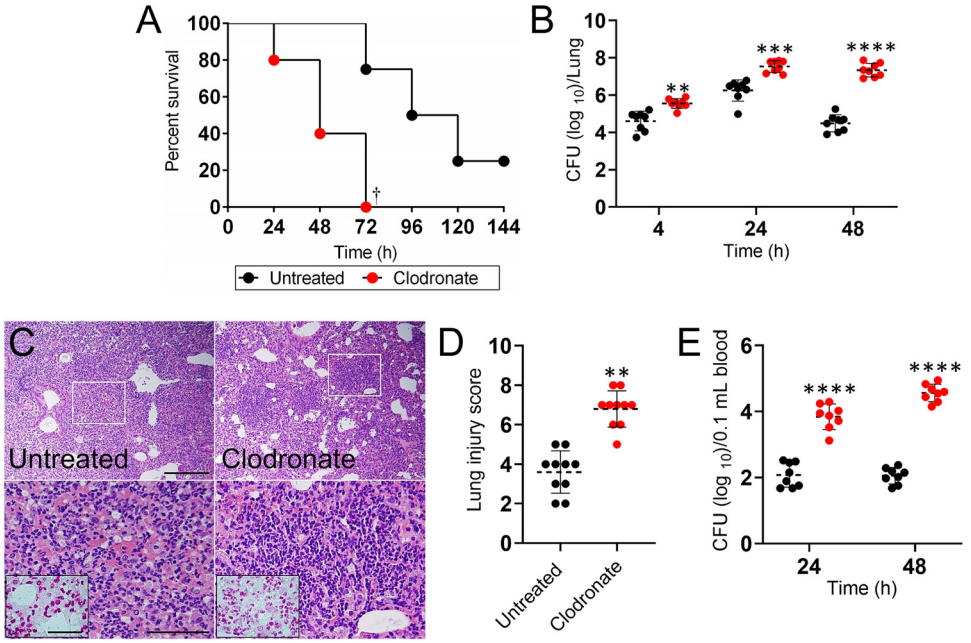

FIG 1 Administration of liposomal clodronate followed by *Acinetobacter baumannii* infection reduces survival in C57BL/6 mice. (A) Survival differences of clodronate- and PBS-injected (untreated) C57BL/6 mice after infection with 5×10^7 *A. baumannii* cells ($n = 5$ per group). Clodronate-treated and uninfected mice were used as additional controls (data not shown; all of the mice in each of these groups survived). Dagger symbol denotes *P* value significance (†, $P < 0.01$) calculated by log rank (Mantel-Cox) analysis. Bacterial burden (CFU) in lungs (B) excised and blood (E) collected from untreated and clodronate-treated mice infected with 10^7 *A. baumannii* cells ($n = 8$ per group) 4 (lungs only), 24, and 48 h postinfection. (C) Histological analysis of lungs removed from untreated and clodronate-treated *A. baumannii*-infected C57BL/6 mice 48 h postinfection. Representative ×10 (upper panel; scale bar, 100 μm) and ×40 (lower panel; scale bar, 20 μm; magnified white boxes in upper panel) magnification of H&E-stained sections of the lungs are shown with Gram staining insets (lower panel; scale bars, 10 μm) showing the Gram-negative *A. baumannii* (pink-red). (D) The lung injury score (LIS) was evaluated blindly by two independent investigators. Each symbol indicates the average score for 5 fields per image per investigator. For panels B, D, and E, dashed lines and error bars denote the means and standard deviations (SDs), respectively. Asterisks denote *P* value significance (**, $P < 0.001$; ***, $P < 0.0001$; ****, $P < 0.00001$) calculated by analysis of variance (ANOVA) and adjusted by use of the Bonferroni correction. Each experiment was performed independently twice, and the data obtained in each experiment were compiled into the graphs shown.

Macrophage depletion increases neutrophil recruitment in lung tissue. We identified macrophage infiltration 48 h postinfection by measuring the expression of F4/80, which is a marker typically expressed and upregulated during the activation of these cells (18). As expected, flow cytometry revealed that lung homogenates of clodronate-treated mice infected with *A. baumannii* showed significantly reduced numbers of F4/80-positive (F4/80$^+$) cells relative to untreated mice ($P < 0.0001$) (Fig. 2A and B). Immunohistochemistry was used to confirm the flow cytometric analysis. Twenty-four hours postinfection, dark staining (red arrows) in tissue sections from untreated murine lungs displayed substantial macrophage recruitment (Fig. 2C). In contrast, clodronate-treated infected mice showed a decrease in macrophage recruitment to the lung area, consistent with macrophage depletion as well as a reduction in the recruitment of clodronate-resistant macrophages. Moreover, macrophage counts 4 and 48 h postinfection revealed that lungs of clodronate-treated mice infected with *A. baumannii* displayed significantly lower numbers of these reticuloendothelial cells than the untreated and infected group ($P < 0.0001$) (Fig. 2D).

We investigated the effect of macrophage depletion on neutrophil migration to the lungs due to the importance of these leukocytes in controlling bacterial infections. Neutrophil infiltration was evaluated by measuring the number of Ly-6G$^+$ cells in the pulmonary tissue 48 h postinfection. Ly-6G is a receptor expressed specifically by neutrophils (19). Flow cytometry analysis of tissue evinced substantially more neutrophils in the lungs of clodronate-treated mice infected with *A. baumannii* than untreated

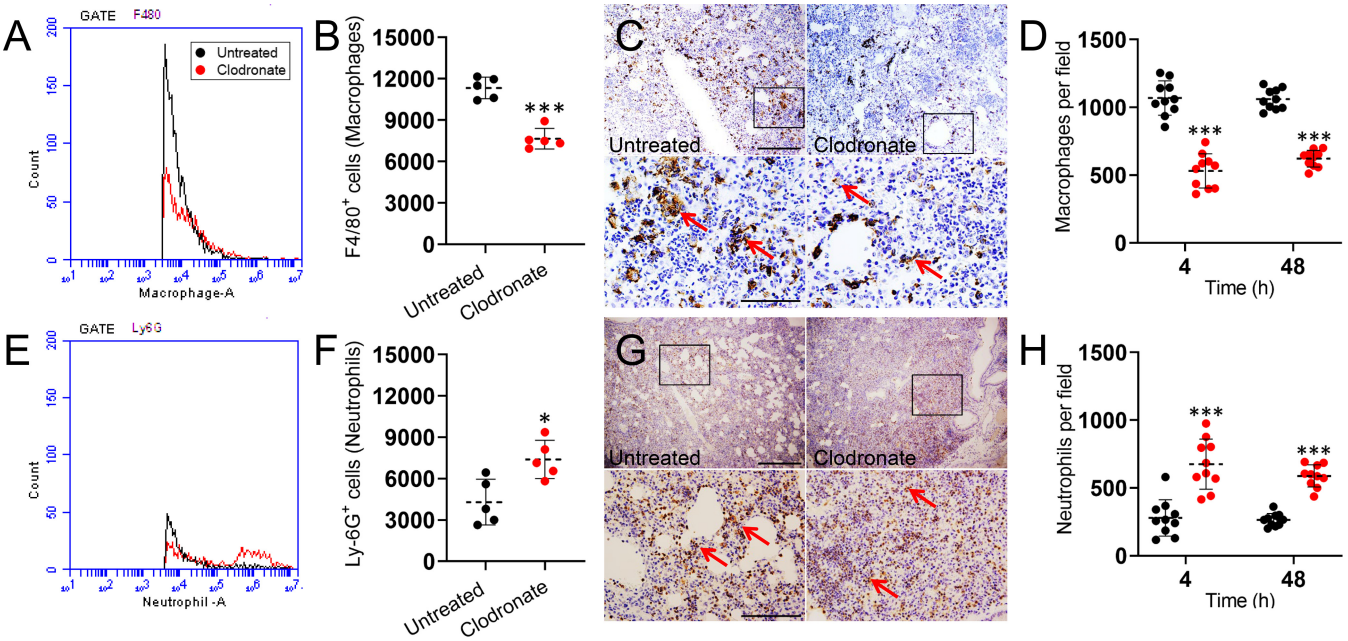

FIG 2 Liposomal clodronate administration alters the number of macrophages and neutrophils in lung tissue of C57BL/6 mice infected with *A. baumannii*. The expression levels of the F4/80$^+$ (macrophages) (A and B) and Ly-6G$^+$ (neutrophils) (E and F) cells in lung homogenates were analyzed by flow cytometry 24 h postinfection. Representative histograms and graphs quantifying the number of F4/80$^+$ and Ly-6G$^+$ cells per condition are shown. Primary cells were isolated from lungs of mice exposed to liposomal PBS (untreated) or clodronate and infected intranasally with 10^7 *A. baumannii* cells. For panels B and F, each symbol represents a mouse ($n = 5$). Representative F4/80 (C) and Ly-6G (G) stained sections of untreated and clodronate-treated lungs are shown (scale bar, 100 μm; $\times$10 magnifications for upper panel; and scale bar, 20 μm; $\times$40 magnification for lower panel) with brown (horseradish peroxidase [HRP]) staining indicating cellular infiltration. Red arrows in the lower high magnification panels indicate F4/80- and Ly-6G-positive cells. Number of macrophages (D) and neutrophils (H) per field in lung tissue of untreated and clodronate-treated animals infected with *A. baumannii* after 4 and 48 h. For panels D and H, each symbol represents a $\times$40 microscopic field of view ($n = 10$ per group). For panels B, D, F, and H, dashed lines indicate the average for each experimental condition, and error bars indicate SDs. Asterisks denote *P* value significance (*, $P < 0.01$; ***, $P < 0.0001$) calculated using ANOVA and adjusted by use of the Bonferroni correction.

animals ($P < 0.01$) (Fig. 2E and F). Additionally, immunohistochemistry confirmed higher infiltration of neutrophils as indicated by the localized dark staining (red arrows) in lung tissue of clodronate-treated mice infected with *A. baumannii* compared to that of untreated control mice (Fig. 2G). Likewise, neutrophil counts 4 and 48 h postinfection demonstrated that the respiratory tissue of clodronate-treated and infected rodents exhibited significantly higher numbers of these granulocytes than the control group ($P < 0.0001$) (Fig. 2H). It was possible that the increased neutrophil abundance simply reflected reduced clearance of dead cells by alveolar macrophages at 24 and 48 h postinfection and not enhanced recruitment to the lung. However, neutrophil counts in the lungs of clodronate-treated animals 4 h after infection demonstrated that there is significantly higher infiltration of these granulocytes compared to that of untreated controls ($P < 0.0001$) (Fig. 2H). Our results showed that depletion of macrophages by clodronate increases bacterial titers (Fig. 1) and influences neutrophil recruitment to alveolae infected with *A. baumannii* (Fig. 2).

Depletion of macrophages reduces cytokine levels in the lungs. Cytokines are essential to the maturation and activity of cells of the immune system, including macrophages. For example, cytokines link innate and adaptive immunity and can influence the macrophage's microenvironment. Therefore, we assessed the impact of macrophage depletion during *A. baumannii* pneumonia on the production of pro- and anti-inflammatory cytokines 4 and 24 h postinfection (Table 1). The pulmonary tissue of infected mice treated with clodronate contained significantly lower quantities of tumor necrosis factor alpha (TNF-α), interleukin-1β (IL-1β), IL-6, and IL-12 than the untreated control group ($P < 0.05$). There were no differences observed in the levels of the anti-inflammatory cytokines, IL-4 and IL-10, between the groups. These findings are consistent with the depletion of macrophages, increase in microbial load, and influx of neutrophils we observed in Fig. 1 and 2.

TABLE 1 Cytokine levels in the lungs of *Acinetobacter baumannii*-infected C57BL/6 mice[a]

Time and group	Cytokine level (avg ± SEM) (pg/ml)[b]					
	TNF-α	IL-1β	IL-4	IL-6	IL-10	IL-12
4 h						
Untreated	814.6 ± 52.1	241.5 ± 14.8	38.89 ± 3.7	3451.7 ± 40.6	129.4 ± 12.3	217.1 ± 4.3
Clodronate	407.8 ± 23.9†	63.17 ± 5.8†	51.37 ± 3.8	381.1 ± 11.2†	126.6 ± 8.4	37.95 ± 9.2†
24 h						
Untreated	541.8 ± 99.4	133.4 ± 20.1	80.28 ± 5.1	613.7 ± 61.4	82.89 ± 18.9	144.2 ± 9.5
Clodronate	208.3 ± 36.8†	57.65 ± 3.2†	93.73 ± 9.7	65.90 ± 25.9†	82.69 ± 9.0	29.66 ± 7.5†

[a]$n = 5$ per group.
[b]†, Lower cytokine levels ($P < 0.05$) than those of the untreated group.

Depletion of macrophages and high bacterial burden promotes production of reactive oxygen species in pulmonary tissue. The increased infiltration of neutrophils suggested additional physiological changes may be present in *A. baumannii*-infected lungs deficient in macrophages. For example, recruitment of neutrophils not only helps in the clearance of pathogens and foreign particles, but overproduction of reactive oxygen species (ROS) by these inflammatory cells may also lead to tissue injury. ROS are key signaling molecules that play an important role in the progression of inflammatory disorders including infection. Therefore, we investigated whether macrophage depletion enhances ROS production in the lungs of *A. baumannii*-infected mice after 24 h. Production of ROS was measured by using 2′,7′-dichlorodihydrofluorescein diacetate (H_2DCFDA), a ROS-sensitive fluorescent dye (Fig. 3A). Images of pulmonary tissue from clodronate-treated and infected mice displayed a considerably higher fluorescent intensity or ROS production than untreated and infected controls ($P < 0.0001$) (Fig. 3A and B). To confirm these findings, we specifically measured the activity of superoxide dismutase in supernatants of lung tissue homogenates of untreated and clodronate-treated rodents infected with *A. baumannii* using a colorimetric assay (Fig. 3C). Pulmonary tissue of clodronate-treated animals showcased significantly higher superoxide dismutase activity compared to that of untreated mice ($P < 0.0001$) (Fig. 3C). To further characterize the effect of neutrophil-induced ROS overproduction during *A. baumannii* infection, cellular toxicity was assessed by measuring lactate dehydrogenase (LDH) release, an indicator of host cell membrane integrity and cell viability, in lung tissue lavage of untreated and clodronate-treated rodents (Fig. 3D). Elevated levels of LDH were found in pulmonary tissue of macrophage-depleted animals compared to those of untreated controls ($P < 0.0001$) (Fig. 3D). Taken together, these results demonstrate the importance of macrophages in controlling bacterial replication and modulating ROS generation during *A. baumannii* infection and, thus, preventing tissue damage in the respiratory system. It is possible that ROS generation in pulmonary tissue is attributed to neutrophils or epithelial cells. Therefore, we focused on investigating neutrophil-induced ROS production in the context of macrophage depletion and *A. baumannii* infection. Since depletion of macrophages and *A. baumannii* growth stimulate the production of ROS and increase the accumulation of LDH in murine pulmonary tissue, we assessed whether *A. baumannii* infection alone, clodronate treatment, or both facilitate pulmonary cellular apoptosis by flow cytometry (Fig. 3E) using annexin V-fluorescein isothiocyanate (FITC; green) and propidium iodine (PI; red). Viable cells with intact membranes exclude PI, whereas the membranes of dead and damaged cells are permeable to PI. Flow cytometry of pulmonary tissue homogenates validated that untreated cells evinced 88.6% viability, 8.2% apoptosis, and 3.1% nonapoptotic death. Lungs of mice infected with *A. baumannii* displayed 36.3% viable, 43.9% apoptotic, and 18.8% nonapoptotic dead cells. Clodronate-treated animals showed 75% viable, 15.5% apoptotic, and 8.8% nonapoptotic dead cells. In contrast, samples from clodronate-treated infected animals demonstrated a significant early apoptotic population, with only 5.7% viable, 53.1% apoptotic, and 39.8% of the population consisting of nonapoptotic dead cells. Together, our findings demonstrate that macrophage depletion and

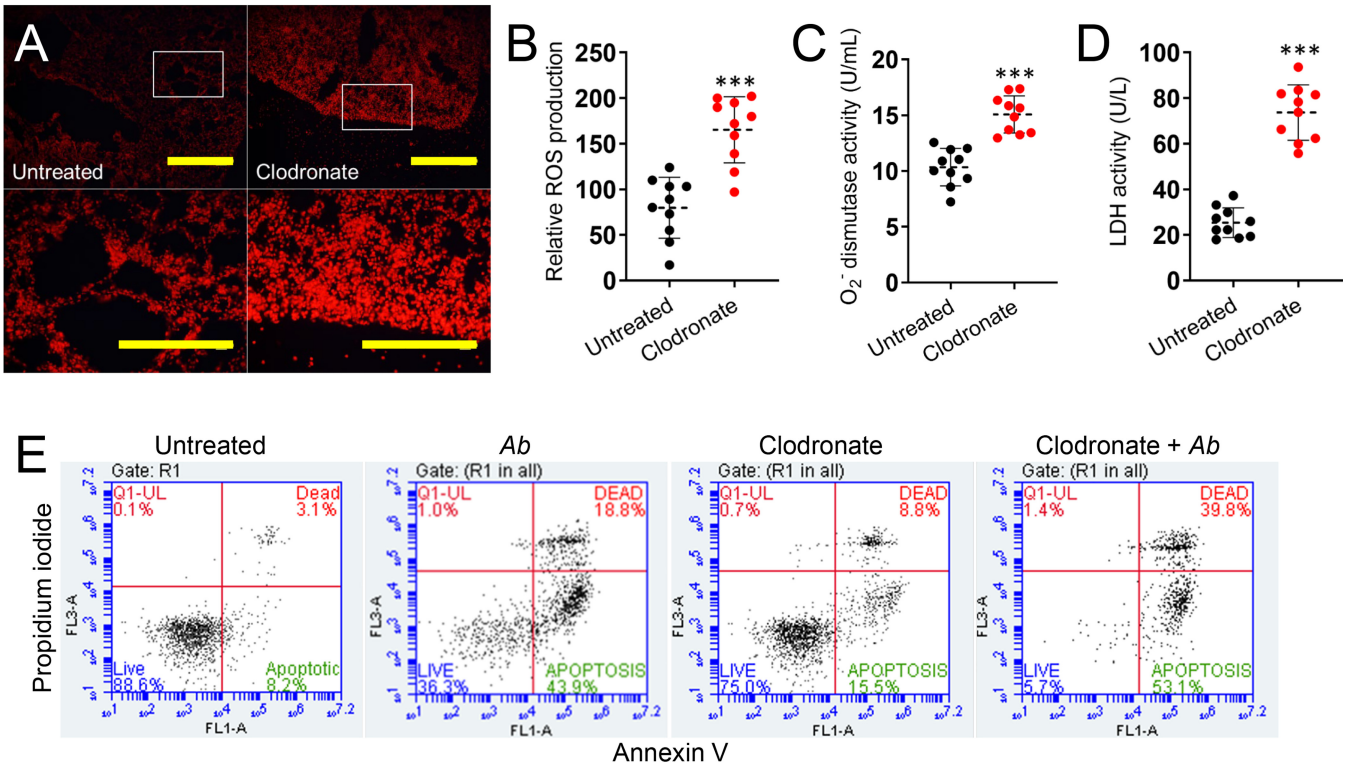

FIG 3 Depletion of macrophages stimulates production of reactive oxygen species (ROS) in pulmonary tissue of C57BL/6 mice infected with *A. baumannii* (*Ab*). (A) Fluorescent images (scale bar, 100 μm; ×10 magnifications for upper panel; and scale bar, 50 μm; ×40 magnification for lower panel or magnified white boxes in upper panel) showing differences in ROS production measured by H_2DCFDA in fresh lung tissue of untreated and clodronate-treated mice infected with *A. baumannii* after 24 h. (B) Relative changes in ROS generation (H_2DCFDA; fluorescence intensity) in living tissue were quantified using Adobe Photoshop CC software. A set of 10 images ($n = 10$ per group) per each field were acquired. (C) Superoxide (O_2^-) dismutase activity was measured in tissue homogenates excised from untreated and clodronate-treated mice infected with *A. baumannii*. (D) Relative lactate dehydrogenase (LDH) activity was measured in the supernatant of pulmonary tissue homogenates of untreated and clodronate-treated animals infected with *A. baumannii*. For panels C and D, each symbol represents a mouse ($n = 10$ per group for O_2^- dismutase and LDH activities). Each experiment was performed independently twice, and the data obtained in each experiment were compiled into the graphs shown. For panels B to D, dashed lines signify the average for each experimental condition, and error bars indicate SDs. Asterisks denote *P* value significance (***, $P < 0.0001$) calculated using Student's *t* test analysis. (E) Macrophage depletion and *A. baumannii* infection induce apoptosis and necrosis of lung cells of C57BL/6 mice. Animals were treated with clodronate, infected with bacteria, or a combination of both, and lung homogenate cells were harvested and compared to cells isolated from untreated animals. Apoptotic cells were analyzed by flow cytometry after being stained with annexin V-FITC together with propidium iodide (PI). Representative percentages of viable (live) and apoptotic or nonapoptotic dead cells for each condition are reported.

infection contribute to cell death *in vivo* by either apoptosis or necrosis in cells of the respiratory system.

Neutrophils release high levels of superoxide during interactions with *A. baumannii*. Since neutrophil ROS and bacterial replication were responsible for pulmonary tissue damage *in vivo* in the absence of regulatory macrophages, we sought to confirm the impact of lipopolysaccharide (LPS), which is extensively released during *A. baumannii* infection (20, 21), on superoxide (O_2^-) dismutase activity, which may result in extracellular O_2^- production by neutrophils. We first validated that LPS is broadly released in culture by the bacterium (Fig. 4A). In addition, we found no differences in LPS shed in culture by *A. baumannii* alone or after incubation with neutrophils, either separated by a membrane (insert) that allowed molecular exchange or in direct contact (Fig. 4A). Then, our results indicate that O_2^- dismutase activity was significantly increased in the supernatants of neutrophils exposed to LPS ($P < 0.0001$) relative to control leukocytes (Fig. 4B). We added the NADPH oxidase inhibitor diphenyleneiodonium (DPI) to prevent O_2^- dismutase activity in neutrophils grown with LPS (20). DPI-treated granulocytes incubated with LPS evinced a decrease in the activity of O_2^- dismutase by ~50%, similar to neutrophils incubated in the absence of endotoxin (Fig. 4B), indicating that neutrophil-mediated oxidative tissue damage is conceivable after macrophage depletion and *A. baumannii* proliferation.

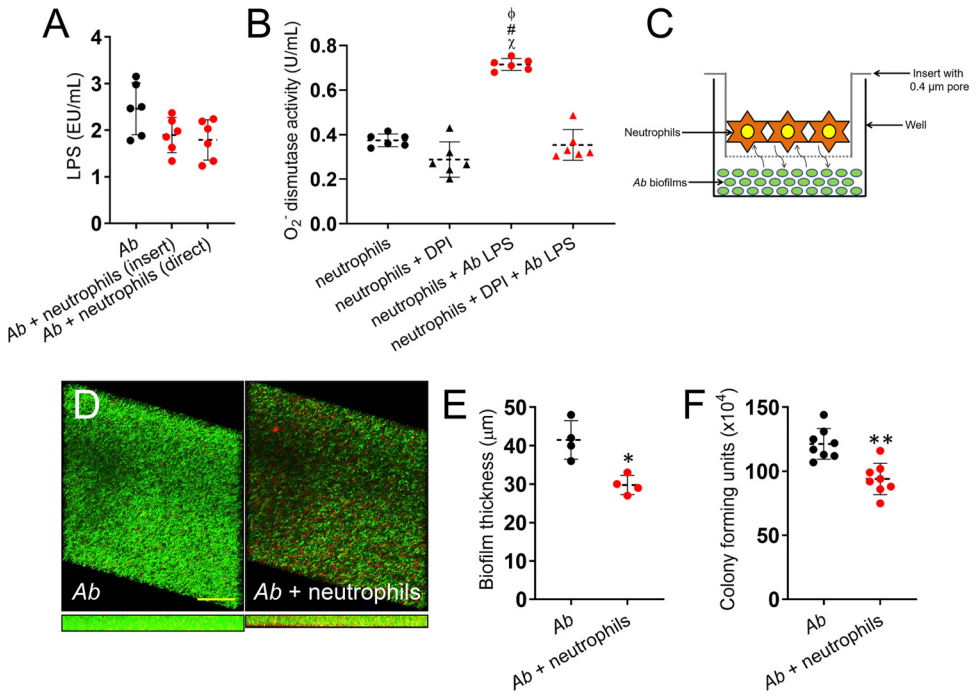

FIG 4 Neutrophils release significant amounts of superoxide after incubation with *A. baumannii* (*Ab*) biofilms and LPS. (A) LPS release from *A. baumannii* strain 0057 after indirect and direct interactions with neutrophils isolated from C57BL/6 mice. (B) Superoxide (O_2^-) dismutase activity was measured in supernatants from neutrophils incubated alone, with O_2^- inhibitor diphenyleneiodonium (DPI), *A. baumannii* LPS, or DPI and LPS. (C) Graphic representation of neutrophils and *A. baumannii* biofilms interaction assay performed in this study. Neutrophils and bacterial biofilms were grown separately (neutrophils, 0.4-μm pore insert; *A. baumannii*, bottom of a well) and coincubated using a microtiter transwell system that permits chemotactic exchange through the supernatant. (D) Confocal microscopy of *A. baumannii* strain 0057 biofilms after interaction with neutrophils. Images of mature bacterial biofilms showed viable (green [SYTO 9]) and dead (red [PI]) cells. The pictures were taken at a magnification of $\times$63. Scale bars, 50 μm. (E) The thickness and morphology of the biofilms can be observed in the *Z*-stack reconstruction. (F) Bacterial viability within biofilms was determined by CFU. For panels A, B, E, and F, each symbol (black or red circles and triangles) represents a technical replicate (panels A and B, $n = 6$; panel E, $n = 4$; panel F, $n = 8$) per condition, dashed lines signify the average for each experimental condition, and error bars indicate SDs. For panel B, symbols (χ, #, ϕ, $P < 0.0001$) denote *P* value significance calculated using ANOVA and adjusted by use of the Bonferroni correction. The symbols χ, #, and ϕ indicate higher O_2^- levels in supernatants of neutrophils plus *A. baumannii* LPS than in neutrophils alone, neutrophils plus DPI, and neutrophils plus DPI plus *A. baumannii* LPS, respectively. For panels E and F, an asterisk denotes *P* value significance (*, $P < 0.01$; **, $P < 0.001$) calculated by Student's *t* test. For panels A, B, and F, each experiment was performed independently twice, and the data obtained in each experiment were compiled into the graphs shown.

To further investigate the impact of neutrophil ROS production in response to *A. baumannii* infection, we next surveyed what effect neutrophils had on formation of bacterial biofilms. Biofilms and neutrophils were grown separately and coincubated using a semipermeable microtiter transwell system that allows chemotactic exchange or the passage of small solutes and proteins through the supernatant (Fig. 4C). Confocal microscopy examination was used to examine the visible effects of the neutrophil effector functions on biofilm structure (Fig. 4D). Regions of green fluorescence (SYTO 9) represent viable cells; the red fluorescence (PI) indicates metabolically inactive or nonviable cells. Control *A. baumannii* strain 0057 biofilms grown in the absence of neutrophils showed a robust architecture, with a thickness of ~41.5 μm and a majority of viable cells encased in an exopolymeric matrix (Fig. 4D and E). Biofilms coincubated with neutrophils exhibited a combination of viable and dead cells, decreased thickness (~29.75 μm), and structural disruption ($P < 0.01$) (Fig. 4D and E). By enumerating CFU, we explored the antimicrobial efficacy of neutrophils on biofilm-associated bacterial viability. On average, *A. baumannii* biofilms interacting with neutrophils demonstrated significantly lower survival than those of control bacteria ($P < 0.001$) (Fig. 4F). Thus, neutrophils may prevent *A. baumannii* infection by reducing bacterial cell viability and biofilm formation.

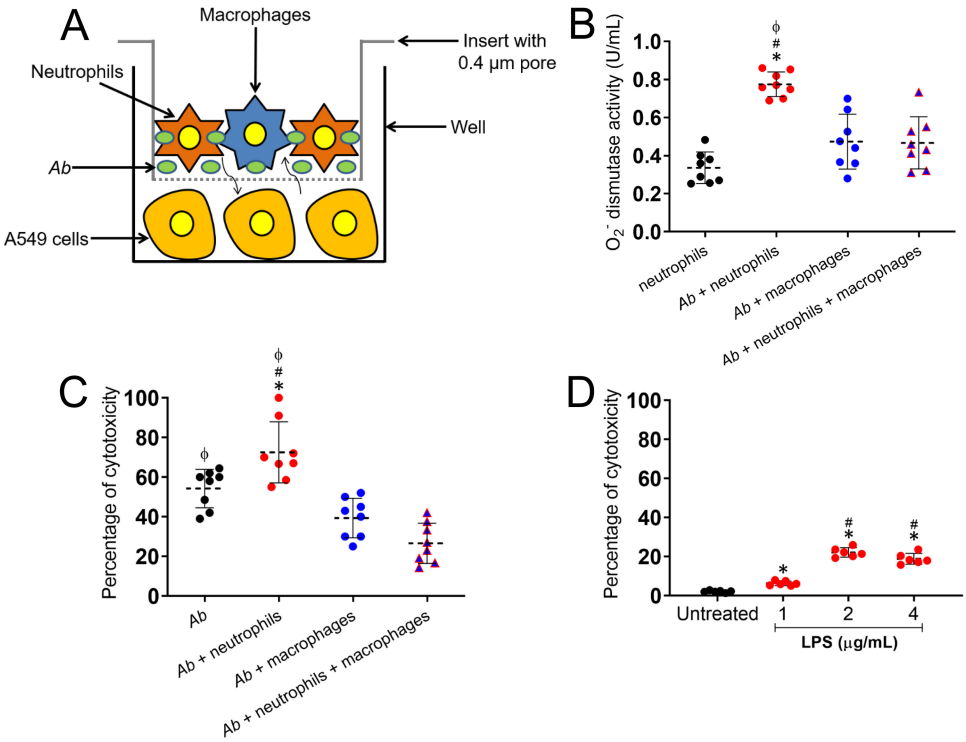

FIG 5 The increased production of O_2^- by neutrophils in the presence of *A. baumannii* is associated with epithelial cell death. (A) Graphic representation of macrophages, neutrophils, and *A. baumannii* (*Ab*) interaction assay. Individual phagocytic cells or coculture and bacteria were coincubated in direct contact on a pore insert, placed on a microtiter well containing A549 epithelial lung cells, and the supernatant collected after each interaction. (B) O_2^- dismutase activity was quantified in culture supernatants. The percentage of cytotoxicity among A549 cells was determined using the trypan blue exclusion test after coincubation with *A. baumannii* and phagocytic cells (C) or LPS (D). For panels B to D, each symbol (black, red, or blue circles and triangles) represents a technical replicate (B and C, $n = 8$; D, $n = 6$) per condition, dashed lines signify the average for each experimental condition, and error bars indicate SDs. Each experiment was performed independently twice, and the data obtained in each experiment were compiled into the graphs shown. For panel B, symbols (*, #, ϕ, $P < 0.0001$) denote *P* value significance calculated using ANOVA and adjusted by use of the Bonferroni correction. Symbols *, #, and ϕ indicate higher O_2^- dismutase activity in supernatants of A549 cells incubated with *A. baumannii* plus neutrophils than in epithelial cells incubated with neutrophils, *A. baumannii* plus macrophages, and *A. baumannii* plus neutrophils plus macrophages, respectively. For panel C, symbols (*, #, ϕ, $P < 0.0001$; ϕ, $P < 0.05$) denote *P* value significance calculated using ANOVA and adjusted by use of the Bonferroni correction. Symbols *, #, and ϕ indicate higher A549 cytotoxicity than *A. baumannii*, *A. baumannii* plus macrophages, and *A. baumannii* plus neutrophils plus macrophages, respectively. For panel D, symbols (*, #, $P < 0.0001$; *, $P < 0.01$) denote *P* value significance calculated using ANOVA and adjusted by use of the Bonferroni correction. Symbols * and # indicate higher A549 cytotoxicity than in untreated and 1 μg/ml LPS-treated cells, respectively.

Neutrophil production of O_2^- and damage of A549 cells are influenced by macrophage reduction and *A. baumannii* replication. Given that macrophage depletion changes the complexion of the immune response within an *A. baumannii*-infected lung, we were curious how existing lung tissue would respond to this change. Therefore, to model these cellular interactions, we investigated the ability of alveolar macrophages to control neutrophils from damaging A549 epithelial lung cells in the presence of *A. baumannii* (Fig. 5). To set up this experiment, a monolayer of A549 cells was first grown separately. Next, using a microtiter transwell system that permits chemotactic exchange through the culture supernatant, the monolayers were coincubated with *A. baumannii* or with *A. baumannii* that was coincubated with phagocytic cells (neutrophils, macrophages, or neutrophils plus macrophages) (Fig. 5A). We then determined the activity of O_2^- dismutase when A549 cells were coincubated with bacteria and phagocytic cells (Fig. 5B). The interaction of neutrophils with *A. baumannii* increases the activity of O_2^- dismutase in the system supernatant compared to that of epithelial cells incubated with neutrophils alone or macrophages with bacteria ($P < 0.0001$). The combined incubation of neutrophils and macrophages with *A. bau-*

mannii showed substantial reduction of O_2^- dismutase activity in the supernatant, suggesting that macrophages play an important regulatory function in either phagocytosing and killing bacteria or modulating neutrophil production of effector molecules such as ROS. Next, we investigated the impact of macrophages on preventing neutrophil-induced damage of A549 epithelial cells using the trypan blue exclusion test of cell viability (Fig. 5C). We found that neutrophils incubated with bacteria caused significant cytotoxic effects on epithelial cells compared to those of macrophages or a phagocytic cell combination ($P < 0.0001$). Interestingly, separate coincubation of A549 cells and *A. baumannii* also resulted in considerably reduced mammalian cell viability (45.75%; $P < 0.05$ relative to *A. baumannii* plus neutrophils), indicating that released molecules by the bacterium such as LPS might have negative effects on epithelial cells of the lungs. This observation is supported by previous studies suggesting that LPS attenuates the inflammatory response (21, 22) and induces apoptosis in epithelial A549 cells through ROS-mediated activation of the intrinsic mitochondrion-cytochrome c-caspase protease mechanism (23). Hence, we directly tested the effect of increasing concentrations (1, 2, and 4 μg/ml) of LPS on the viability of A549 cells (Fig. 5D). We observed significant cytotoxicity in epithelial cells incubated with 2 (22.1%) and 4 (18.9%) μg/ml of LPS compared to that of the untreated (2.1%) or 1 μg/ml (6.3%) of LPS-treated cells ($P < 0.0001$). Also, A549 cells treated with 1 μg/ml of LPS exhibited significantly higher cytotoxicity than untreated cells ($P < 0.01$). Therefore, we concluded that epithelial cell toxicity results from increased neutrophil O_2^- superoxide dismutase activity, O_2^- overproduction, and bacterial replication.

DISCUSSION

During *A. baumannii* pneumonia, immunocompetent C57BL/6 mice demonstrate substantial infiltration and activation of macrophages into bronchoalveolar spaces (16), leading to invasion of the bloodstream. We validated that depletion of alveolar macrophages significantly enhances the susceptibility of mice to *A. baumannii* pneumonia (16, 24). Similar to a previous study using a leukopenic murine model of *A. baumannii* infection (25), the histopathology of clodronate-treated lungs infected with *A. baumannii* revealed a high injury score with consolidated or abscess-like regions characterized by extensive infiltration of polymorphonuclear leukocytes and high numbers of bacteria. In this regard, we observed a significant presence of *A. baumannii* in the bloodstream of macrophage-depleted mice after 24 h of infection resulting in high mortality. The lethality of bloodstream *A. baumannii* infections in mice is driven by the interaction between bacterial LPS and host TLR-4-mediated sepsis pathways (26).

We found that depletion of alveolar macrophages in the lungs enhances bacterial replication and increases the influx of neutrophils to the sites of *A. baumannii* infection. Macrophages are necessary for regulation of neutrophil recruitment (27, 28), and their absence substantially promotes *A. baumannii* growth and colonization of the pulmonary tissue (16). Neutrophils play an important role in early control of acute *A. baumannii* infection by killing bacteria through powerful oxidative and nonoxidative mechanisms and the production of proinflammatory cytokines (29). Upon *A. baumannii* respiratory infection and growth, the numbers of neutrophils increase within the pulmonary capillaries. The inability of neutrophils to penetrate *A. baumannii* biofilms may also prolong their presence in respiratory tissue, intensifying ROS-mediated collateral damage to local tissue, affecting function, and resulting in death of the host. Histological sections of clodronate-treated lungs showcased high ROS production, massive cellular infiltration with minimal alveolar spaces, and high bacterial load. This is consistent with elevated superoxide dismutase activity (and concomitant ROS production) in lung tissue of macrophage-depleted mice (30). In fact, recent studies indicate that *A. baumannii* actively regulates transcriptional responses to oxidative stress facilitating its survival in the lungs (31, 32). Aligned with these findings, our studies revealed that alveolar macrophage depletion and *A. baumannii* infection promote apoptosis and necrosis in pulmonary cells.

Neutrophils constitutively die by apoptosis at inflammatory sites and are ingested

by macrophages (33, 34). During apoptosis, neutrophil surface membranes remain intact, containing their potentially injurious cytoplasmic contents. If apoptotic and death neutrophils are not efficiently cleared, these programmed leukocytes further degrade and leak their intracellular proteases into the alveolar spaces, producing more tissue injury and perpetuating inflammation. Neutrophil clearance interrupts the release of inflammatory mediators (34, 35), and processing of apoptotic cells accelerates resolution of inflammation (36). Changes in membrane surface markers of the apoptotic neutrophils target them for phagocytosis and clearance by alveolar macrophages (37). Macrophage-depleted rodents infected with *A. baumannii* are likely unable to eradicate bacteria, eliminate apoptotic neutrophils, or prevent the influx of newly stimulated neutrophils from infected respiratory tissue, resulting in detrimental dwelling of these leukocytes and extensive alveolar capillary injury. It is also possible that macrophages inhibit neutrophils through a juxtacrine/paracrine signaling event. However, this is an area of future investigation and out of the scope of the current study.

In order to elucidate the role that neutrophils play in tissue damage due to the absence of regulatory macrophages, we studied the antimicrobial functions of neutrophils other than phagocytosis on *A. baumannii* biofilms after separation using a membrane that only permits chemotactic exchange. Superoxide dismutase activity in neutrophils was significantly increased in response to bacterial LPS release. However, although the effector molecules of neutrophils caused notable damage to *A. baumannii* biofilms, the resident bacterial load was diminished but not completely eradicated. It is possible that during direct interaction in tissue, biofilm formation protects individual bacterial cells from immune cells and antimicrobial molecules. This helps explain why control and elimination of *A. baumannii* infections is often so difficult. *A. baumannii* can adhere to neutrophils and use these phagocytic cells as a mechanism of transport in a process modulated by IL-8 production (38). This described interaction may play an important role in dissemination of biofilm-associated bacteria in tissue to other organs. Interestingly, biofilm-related bacteria in endotracheal tubes of patients in prolonged mechanical ventilation interact with neutrophils in respiratory secretions, suggesting that these leukocytes may facilitate systemic bacterial propagation (39). Furthermore, this process has been associated with low levels of proinflammatory cytokines such as TNF-α, IL-1β, IL-6, and IL-12, which is similar to the environment, observed in clodronate-treated mice (38). These findings highlight the importance of macrophages as modulators of the immune response in infections by Gram-negative bacteria (40).

LPS is extensively released by virulent *A. baumannii* strains during infection (26, 41) and reduces the expression of pattern recognition receptor CD14 on the surface of human neutrophils (42). We found that *A. baumannii* actively releases LPS when incubated with neutrophils, and these leukocytes responded by increasing the activity of O_2^- dismutase, an indication of high O_2^- production. This result supports the observation in the murine model that the depletion of macrophages during *A. baumannii* infection leads to high bacterial titers, the intensification of neutrophil infiltration to pulmonary tissue, and stimulates the production of ROS-mediated tissue damage. Likewise, *A. baumannii* LPS induces the activation of the TLR-4 pathway, which was previously shown to cause septic shock and death in mice (26). As a proof of concept, we used a flexible tissue culture system in which epithelial cells were separated from the interaction between *A. baumannii* and phagocytic cells. Our findings indicate that interaction of neutrophils with the bacterium induces the production of high levels of O_2^- and cell death.

Finally, *A. baumannii*-shed molecules had detrimental effects on A549 epithelial cells. Although outside of the scope of this study, it would be interesting to determine which molecules other than LPS are responsible for these negative effects. It is important to mention that similar effects have been observed in interactions of the bacterium with the fungus *Cryptococcus neoformans*, suggesting that a close analysis of metabolites released by *A. baumannii* in aqueous medium may be important to understand its pathogenesis (43). Future studies are warranted to understand the effect

of *A. baumannii* metabolites on epithelial cells of the respiratory system as well as on the function of phagocytic cells.

MATERIALS AND METHODS

Acinetobacter baumannii. *A. baumannii* strain 0057, a clinical isolate that was generously provided by Mark D. Adams (Cleveland, OH), was chosen for this study because it has been sequenced and is resistant to multiple antibiotics commonly used to treat Gram-negative infections. The strain was first collected from the bloodstream of a soldier in 2004 at Walter Reed Army Medical Center, Washington, DC. The strain was stored at −80°C in brain heart infusion (Becton, Dickinson [BD] Biosciences) broth with 40% glycerol until use. The organism was propagated in the laboratory by growth in tryptic soy broth (MP Biomedicals) overnight at 37°C using an orbital shaker set at 150 rpm. Growth was monitored by measuring the optical density (OD) at 600 nm using a microtiter plate reader (BioTek).

Human epithelial cells. The human type II alveolar epithelial cell-like cell line A549 (ATCC) was used in this study. These cells are derived from lung carcinomatous tissue and are widely used in cell models to study infection by respiratory pathogens (44). The cell cultures were maintained as previously described (45, 46).

Ethics statement. All animal studies were conducted according to the experimental practices and standards approved by the Institutional Animal Care and Use Committee at Long Island University (protocol number 11-3).

Depletion of murine alveolar macrophages. Female C57BL/6 mice (6 to 8 weeks; Charles Rivers) were anesthetized with a 100 mg ketamine/kg body weight (Ketaset) and 10 mg/kg xylazine (AnaSed) cocktail followed by intranasal (i.n.) administration of a single dose of 100 μl of liposome-encapsulated dichloromethylene diphosphonate (clodronate; FormuMax Scientific). Control animals were challenged with liposomes containing phosphate-buffered saline (PBS). Forty-eight hours after liposomal administration, macrophage depletion was first assessed by differential leukocyte count of mouse bronchoalveolar lavage using a Hema 3 stat pack (Thermo Fisher) and light microscopy and then confirmed that 85% of alveolar macrophages were depleted using flow cytometry as described below.

Bacterial infection. Clodronate- and control liposome-treated mice were anesthetized 48 h after treatment, and sublethal infections were induced by i.n. inoculation of a suspension containing approximately 10^7 *A. baumannii* cells. For survival studies, lethal infection was performed by i.n. inoculation with 5×10^7 bacteria. To monitor the impact of alveolar macrophages in mouse survival, clodronate- and saline liposome-treated uninfected animals were used as additional controls. Four animals per group were euthanized 24 and 48 h after infection. Tissues were collected for histological processing and CFU and cytokine production determinations.

CFU determinations in lung tissue and blood. At 24 and 48 h postinfection, mouse lung tissues were excised and homogenized in sterile PBS. Likewise, mouse blood was collected from the retro-orbital sinus using a Pasteur pipette. Serial dilutions of homogenates or blood were performed; a 100-μl suspension of each sample was then plated on tryptic soy agar (TSA; MP Biomedical) plates and incubated at 37°C for 24 h. Quantification of viable bacterial cells was determined by CFU counts, and the results were normalized per lung or blood volume.

Flow cytometry analysis. For flow cytometry staining, primary cells were isolated from excised lung tissue from five mice treated with clodronate or PBS liposomes as described above; the cells were washed and then stained with fluorescence (FITC)-labeled antibodies. Anti-F4/80 (macrophages) or Ly-6G (neutrophils)-FITC (green) and their corresponding isotype controls were purchased (BD). Samples (10,000 events per sample) were processed on a BD Accuri C6 flow cytometer and were analyzed using the FCS express software.

Histological processing, light microscopy, and phagocyte counts. Wounded tissues were excised from euthanized mice; the tissues were fixed in 10% formalin and embedded in paraffin. Four micrometer vertical sections were cut and then fixed to glass slides and subjected to hematoxylin and eosin (H&E) and Gram staining or F4/80 and Ly-6G (conjugated to horseradish peroxidase [HRP]; BD) immunostaining to assess tissue morphology and bacterial burden (red-pink) or macrophage and neutrophil infiltration (brown), respectively. The slides were visualized using an Axiovert 40 CFL inverted microscope (Carl Zeiss), and images were captured with an AxioCam MRc digital camera using the Zen 2011 digital imaging software. The infiltration of macrophages and neutrophils to pulmonary tissue was quantified by cell counts using the recorded ×40 images. Three different people blindly counted 10 fields per condition, and the average result is presented.

Lung injury score. The lung injury score (LIS) was quantified by two investigators blinded to the treatment groups using published criteria by the American Thoracic Society (47). The LIS was obtained by the sum of each of the following six independent variables: neutrophils in the alveolar spaces and/or in the interstitial spaces, presence of hyaline membranes, proteinaceous debris filling the airspaces, alveolar septal thickening, and alveolar congestion. This sum was weighted according to the relevance ascribed to each feature by the American European Consensus Committee (47) and then was normalized to the number of fields evaluated and arbitrarily multiplied by 10 to obtain continuous values between zero and ten (both inclusive). The resulting LIS was derived from the following calculation: $\text{LIS} = \{[(20 \times \text{A}) + (14 \times \text{B}) + (6 \times \text{C}) + (6 \times \text{D}) + (2 \times \text{E}) + (2 \times \text{F})]/(\text{number of fields} \times 100)\} \times 10$.

Cytokine assays. Supernatants from lung homogenates were processed as described above and stored at −80°C until tested. TNF-α, IL-1β, IL-4, IL-6, IL-10, and IL-12 were quantified by enzyme-linked immunosorbent assay (ELISA) (BD) in quadruplets per sample. The limits of detection were 7.8 pg/ml for IL-4; 15.6 pg/ml for TNF-α, IL-1β, and IL-6; 31.3 pg/ml for IL-10; and 62.5 pg/ml for IL-12p70r. Cytokine levels in untreated and clodronate-treated tissue infected with *A. baumannii* were calculated after

subtracting the values obtained from those of the negative control tissue (untreated or clodronate-treated uninfected rodents).

Measurement of ROS *in vivo*. ROS production was measured in pulmonary tissue by H_2DCFDA (Sigma), as previously described (48), 24 h postinfection. Tissues from untreated and clodronate-treated C57BL/6 mice were excised, freshly cut in 5-μm vertical sections using a microtome (Leica), mounted on a slide, and incubated in the dark with H_2DCFDA (10 μM) for 30 min. A set of 10 images per each field was acquired at $\times$10 and $\times$40 magnification using fluorescence microscopy and images captured and processed as described above. Then, semiquantitative analyses were performed to detect changes in H_2DCFDA fluorescence intensity (excitation wavelength, 488 nm; emission wavelength, 515 nm) or ROS production in living tissue using Adobe Photoshop CC software.

LDH measurement. The release of LDH from A549 cells into the medium was monitored as a measure of cell damage. LDH in the pulmonary lavage of untreated and clodronate-treated mice either uninfected or infected with *A. baumannii* was measured by an LDH cytotoxicity assay kit (Cayman Chemical). Lavage from tissues of naive mice processed under identical conditions was included as a negative control. The LDH released by untreated and clodronate-treated tissue infected with bacteria was determined after subtracting the values obtained from those of the negative control tissue. Samples were freshly tested in five wells per condition.

Apoptosis assay. Apoptosis in lung tissue was analyzed by flow cytometry using an annexin V-FITC and PI kit (BD). Pulmonary cells of uninfected, *A. baumannii*-infected, clodronate-treated, and clodronate-treated and *A. baumannii*-infected animals were isolated from lung tissue after homogenization, harvested on ice, washed twice with cold PBS, and resuspended in binding buffer. Five microliters of annexin V-FITC and PI were added to the cells. Each suspension was gently vortexed and incubated for 15 min at room temperature (RT) (25°C) in the dark. Then, 400 μl of binding buffer was added to each tube and samples (10,000 events per sample) were analyzed by flow cytometry within 1 h using a BD Accuri C6 flow cytometer. The percentage of pulmonary cells positive for PI (red) and/or annexin V-FITC (green) was determined using the FCS Express software.

Isolation of neutrophils from mouse bone marrow. Murine bone marrow neutrophils from femurs and tibias were isolated as previously described (49). Briefly, C57BL/6 mice were euthanized, and the animal surface was sprayed with 70% ethanol. An incision was made in the mid-abdomen on the ventral side and the skin removed in order to expose the abdomen and lower extremities. The muscles from both legs were removed using scissors and the acetabulum carefully dislocated from the hip joint. After separating the bones, they were placed in a sterile petri dish containing ice-cold RPMI 1640 medium (feeding medium; Cellgro) supplemented with 10% fetal calf serum (FCS) (Atlanta Biologicals) and 1% penicillin-streptomycin. Each bone was sterilized by rinsing in a 70% ethanol solution followed by three washes in ice-cold sterile PBS. The epiphyses of the bones were cut off and, using a 25-gauge needle and a 12-ml syringe, filled with feeding medium additionally supplemented with 2 mM EDTA (Sigma). The bone marrow cells were flushed onto a 50-ml conical tube through a 100-μm cell strainer. Then, cells were collected by centrifugation at 1,652 rpm for 7 min at 4°C and washed 2$\times$ with feeding medium. Neutrophils were separated from the remaining cells by centrifugation over discontinuous Histopaque 1119 and 1077 (densities, 1.119 and 1.077 g/ml; Sigma) gradients at 2,360 rpm for 30 min at RT. Recovered neutrophils ($>$95 and $\sim$98% as determined by trypan blue staining and flow cytometry using Ly-6G as a marker, respectively) were washed twice with feeding medium, centrifuged at 1,400 rpm for 7 min at 4°C, and cultured in feeding medium for 2 h at 37°C and 5% CO_2.

Isolation of murine alveolar macrophages. Alveolar macrophages were isolated from the lungs of C57BL/6 mice as previously described (50). Briefly, the trachea was exposed, and the lungs were lavaged 10$\times$ with 0.8 ml of sterile calcium and magnesium-free Hanks balanced salt solution (HBSS) supplemented with 1 mM EGTA (Sigma). The bronchoalveolar lavage was centrifuged, resuspended in cell culture medium, and allowed to adhere to 24-well tissue culture plates for 2 h at 37°C in 5% CO_2. The cells were treated with a hypotonic solution of NH_4Cl for 10 min on ice to remove red blood cells. Macrophages were detached from tissue culture plates after trypsin treatment for 30 s. Recovered macrophages ($>$95 and $\sim$98% as determined by trypan blue staining and flow cytometry using F4/80 as a marker, respectively) were washed twice with feeding medium, centrifuged at 1,400 rpm for 7 min at 4°C, and cultured in feeding medium at 37°C in 5% CO_2.

Determination of endotoxin-releasing activity. To quantify the amount of endotoxin released from *A. baumannii* after direct and indirect interaction with neutrophils, we performed a *Limulus* amebocyte lysate (LAL) assay (Lonza) according to the manufacturer's instructions. Briefly, *A. baumannii* (10^6 CFU) was directly or indirectly (separated by a transwell membrane of 0.4 μm) incubated with 10^5 murine neutrophils at RT for 4 h. *A. baumannii* grown alone and commercially available LPS (Sigma) were used as controls. Then, the samples were centrifuged (3,000 rpm) for 1 min. The supernatant was collected and incubated with LAL reagent. The level of endotoxin was determined by measuring the OD at 340 nm on a spectrophotometer (BioTek).

Measurement of superoxide dismutase activity using a colorimetric assay. (i) *In vivo*. Pulmonary tissues of untreated and clodronate-treated mice were excised, weighed, rinsed with PBS with protease inhibitors (Roche), and homogenized in 5 ml of cold 20 mM HEPES buffer (pH 7.2) containing 1 mM EGTA, 210 mM mannitol, and 70 mM sucrose per gram of tissue. Cell debris was removed from homogenates by centrifugation at 7,200 rpm for 5 min at 4°C. The activity of superoxide (O_2^-) dismutase in murine tissue supernatant was quantified after exposure to *A. baumannii* using a O_2^- dismutase colorimetric assay kit (Cayman Chemical), based on the ability of enzyme to dismutation of O_2^- generated during the xanthine/xanthine oxidase reaction, using a tetrazolium salt as an indicator. Tissues of untreated and uninfected mice (naive) processed under identical conditions were included as negative controls. The

activity of O_2^- dismutase in untreated and clodronate-treated tissue infected with bacteria was determined after subtracting the values obtained from those of the naive control tissue. Samples were freshly tested in five wells per condition.

(ii) *In vitro*. The O_2^- dismutase activity in culture supernatant was quantified after exposure of 10^5 neutrophils to *A. baumannii* LPS, O_2^- inhibitor DPI (10 μg/ml; Sigma), or a combination using the same kit as described above following the manufacturer's recommendations for the management of tissue homogenate supernatant (Fig. 4B). Untreated neutrophils were included as negative controls. Also, the activity of O_2^- dismutase was determined as described above after neutrophils (10^5), macrophages (10^5), or cocultures (10^5 cells per leukocyte) were incubated with *A. baumannii* (10^6 CFU) on an insert with a pore size of 0.4 μm (Corning) that was placed onto a 24-well polystyrene plate containing 10^5 A549 epithelial lung cells in feeding medium and incubated for 12 h at 37°C in 5% CO_2 (Fig. 5A). Cells or debris were removed from supernatant by centrifugation at 7,200 rpm for 5 min at 4°C. Samples were freshly tested in triplicates (Fig. 4B) and quadruplets (Fig. 5B).

Confocal microscopy. The integrity of *A. baumannii* biofilms coincubated in absence or presence of neutrophils was examined using the LIVE/DEAD biofilm viability kit (Invitrogen) and confocal microscopy. *A. baumannii* biofilms were grown for 24 h at 37°C in 35-mm glass-bottom culture dishes (MatTek), coincubated with or without neutrophils in feeding medium for 12 h at 37°C and 5% CO_2, rinsed 3× with distilled water (dH_2O), and incubated for 30 min at RT in 2 ml of dH_2O containing the fluorescent stains SYTO 9 (6 μl) and PI (6 μl) with protection from light. The dishes were then rinsed 3× with dH_2O to remove excess stain. SYTO 9 (excitation wavelength, 500 nm; emission wavelength, 535 nm) labels live and dead bacteria, while PI (excitation wavelength, 600 nm; emission wavelength, 650 nm) penetrates only bacteria with damaged membranes. PI binds to the cell's nucleic acids with greater affinity than SYTO 9. Thus, with the appropriate mixture of the dyes, bacteria with intact cell membranes stain fluorescent green, whereas bacteria with damaged membranes stain fluorescent red. Microscopic examinations of biofilms formed in culture plates were performed with confocal microscopy using an inverted Leica TCS SP5 confocal laser scanning microscope (Leica).

Trypan blue exclusion test of cell viability. After A549 epithelial cells were coincubated with *A. baumannii* and phagocytic cells (neutrophils, macrophages, or neutrophils plus macrophages), the medium was removed, cells were trypsinized, harvested by centrifugation (1,200 rpm, 5 min), and resuspended in PBS to a concentration of 10^5 cells per milliliter (51). Each sample was mixed with an equal volume of 0.4% (wt/vol) trypan blue, and the mixture transferred to a hemocytometer where cells that picked up the dye where considered dead. The percentage of cytotoxicity was calculated by counting 100 cells per field ($n = 4$). Finally, the average of each condition was compared relative to that of control cells.

Statistical analysis. All data were subjected to statistical analysis using GraphPad Prism 7.0 (GraphPad Software). *P* values for multiple comparisons were calculated by analysis of variance (ANOVA) and were adjusted by use of the Bonferroni correction. *P* values for individual comparisons were calculated using Student's *t* test analysis. *P* values of <0.05 were considered significant.

ACKNOWLEDGMENTS

We thank Alice O'Connor at NYIT COM for her helpful contribution to the histological analyses.

M.R.D. was partially supported by the Hofstra University startup funds and Hofstra faculty research and development grant. N.W.R. was supported by the National Science Foundation under award number 1615822. L.R.M. and M.R.D. are supported by the National Institute of Allergy and Infectious Diseases of the U.S. National Institutes of Health (NIH) under award number R01AI145559.

All authors contributed to the project design and experimental procedures, analyzed data, provided the figure presentation, and contributed to manuscript writing.

We declare no conflict of interest.

REFERENCES

1. Howard A, O'Donoghue M, Feeney A, Sleator RD. 2012. *Acinetobacter baumannii*: an emerging opportunistic pathogen. Virulence 3:243–250. https://doi.org/10.4161/viru.19700.
2. Johnson EN, Burns TC, Hayda RA, Hospenthal DR, Murray CK. 2007. Infectious complications of open type III tibial fractures among combat casualties. Clin Infect Dis 45:409–415. https://doi.org/10.1086/520029.
3. Mihu MR, Martinez LR. 2011. Novel therapies for treatment of multi-drug resistant *Acinetobacter baumannii* skin infections. Virulence 2:97–102. https://doi.org/10.4161/viru.2.2.15061.
4. Dijkshoorn L, Nemec A, Seifert H. 2007. An increasing threat in hospitals: multidrug-resistant *Acinetobacter baumannii*. Nat Rev Microbiol 5:939–951. https://doi.org/10.1038/nrmicro1789.
5. Orsinger-Jacobsen SJ, Patel SS, Vellozzi EM, Gialanella P, Nimrichter L, Miranda K, Martinez LR. 2013. Use of a stainless steel washer platform to study *Acinetobacter baumannii* adhesion and biofilm formation on abiotic surfaces. Microbiology 159:2594–2604. https://doi.org/10.1099/mic.0.068825-0.
6. Wendt C, Dietze B, Dietz E, Ruden H. 1997. Survival of *Acinetobacter baumannii* on dry surfaces. J Clin Microbiol 35:1394–1397. https://doi.org/10.1128/JCM.35.6.1394-1397.1997.
7. Tomaras AP, Dorsey CW, Edelmann RE, Actis LA. 2003. Attachment to and biofilm formation on abiotic surfaces by *Acinetobacter baumannii*: involvement of a novel chaperone-usher pili assembly system. Microbiology 149:3473–3484. https://doi.org/10.1099/mic.0.26541-0.
8. Vidal R, Dominguez M, Urrutia H, Bello H, Gonzalez G, Garcia A, Zemelman R. 1996. Biofilm formation by *Acinetobacter baumannii*. Microbios 86:49–58.
9. Aron AT, Heffern MC, Lonergan ZR, Vander Wal MN, Blank BR, Spangler

B, Zhang Y, Park HM, Stahl A, Renslo AR, Skaar EP, Chang CJ. 2017. *In vivo* bioluminescence imaging of labile iron accumulation in a murine model of *Acinetobacter baumannii* infection. Proc Natl Acad Sci U S A 114:12669–12674. https://doi.org/10.1073/pnas.1708747114.
10. Echenique JR, Arienti H, Tolmasky ME, Read RR, Staneloni RJ, Crosa JH, Actis LA. 1992. Characterization of a high-affinity iron transport system in *Acinetobacter baumannii*. J Bacteriol 174:7670–7679. https://doi.org/10.1128/jb.174.23.7670-7679.1992.
11. Harding CM, Hennon SW, Feldman MF. 2018. Uncovering the mechanisms of *Acinetobacter baumannii* virulence. Nat Rev Microbiol 16:91–102. https://doi.org/10.1038/nrmicro.2017.148.
12. Bruhn KW, Pantapalangkoor P, Nielsen T, Tan B, Junus J, Hujer KM, Wright MS, Bonomo RA, Adams MD, Chen W, Spellberg B. 2015. Host fate is rapidly determined by innate effector-microbial interactions during *Acinetobacter baumannii* bacteremia. J Infect Dis 211:1296–1305. https://doi.org/10.1093/infdis/jiu593.
13. Breslow JM, Meissler JJ, Jr, Hartzell RR, Spence PB, Truant A, Gaughan J, Eisenstein TK. 2011. Innate immune responses to systemic *Acinetobacter baumannii* infection in mice: neutrophils, but not interleukin-17, mediate host resistance. Infect Immun 79:3317–3327. https://doi.org/10.1128/IAI.00069-11.
14. van Faassen H, KuoLee R, Harris G, Zhao X, Conlan JW, Chen W. 2007. Neutrophils play an important role in host resistance to respiratory infection with *Acinetobacter baumannii* in mice. Infect Immun 75:5597–5608. https://doi.org/10.1128/IAI.00762-07.
15. Grguric-Smith LM, Lee HH, Gandhi JA, Brennan MB, DeLeon-Rodriguez CM, Coelho C, Han G, Martinez LR. 2015. Neutropenia exacerbates infection by *Acinetobacter baumannii* clinical isolates in a murine wound model. Front Microbiol 6:1134. https://doi.org/10.3389/fmicb.2015.01134.
16. Qiu H, KuoLee R, Harris G, Van Rooijen N, Patel GB, Chen W. 2012. Role of macrophages in early host resistance to respiratory *Acinetobacter baumannii* infection. PLoS One 7:e40019. https://doi.org/10.1371/journal.pone.0040019.
17. Arango Duque G, Descoteaux A. 2014. Macrophage cytokines: involvement in immunity and infectious diseases. Front Immunol 5:491. https://doi.org/10.3389/fimmu.2014.00491.
18. Martinez-Pomares L, Platt N, McKnight AJ, da Silva RP, Gordon S. 1996. Macrophage membrane molecules: markers of tissue differentiation and heterogeneity. Immunobiology 195:407–416. https://doi.org/10.1016/S0171-2985(96)80012-X.
19. Fleming TJ, Fleming ML, Malek TR. 1993. Selective expression of Ly-6G on myeloid lineage cells in mouse bone marrow. RB6-8C5 mAb to granulocyte-differentiation antigen (Gr-1) detects members of the Ly-6 family. J Immunol 151:2399–2408.
20. Hampton MB, Kettle AJ, Winterbourn CC. 1996. Involvement of superoxide and myeloperoxidase in oxygen-dependent killing of *Staphylococcus aureus* by neutrophils. Infect Immun 64:3512–3517. https://doi.org/10.1128/IAI.64.9.3512-3517.1996.
21. Feng T, Yunfeng N, Jinbo Z, Zhipei Z, Huizhong Z, Li L, Tao J, Yunjie W. 2010. Single immunoglobulin IL-1 receptor-related protein attenuates the lipopolysaccharide-induced inflammatory response in A549 cells. Chem Biol Interact 183:442–449. https://doi.org/10.1016/j.cbi.2009.11.022.
22. Zhang A, Yan X, Li H, Gu Z, Zhang P, Zhang H, Li Y, Yu H. 2014. TMEM16A protein attenuates lipopolysaccharide-mediated inflammatory response of human lung epithelial cell line A549. Exp Lung Res 40:237–250. https://doi.org/10.3109/01902148.2014.905655.
23. Chuang CY, Chen TL, Cherng YG, Tai YT, Chen TG, Chen RM. 2011. Lipopolysaccharide induces apoptotic insults to human alveolar epithelial A549 cells through reactive oxygen species-mediated activation of an intrinsic mitochondrion-dependent pathway. Arch Toxicol 85:209–218. https://doi.org/10.1007/s00204-010-0585-x.
24. Tsuchiya T, Nakao N, Yamamoto S, Hirai Y, Miyamoto K, Tsujibo H. 2012. NK1.1$^+$ cells regulate neutrophil migration in mice with *Acinetobacter baumannii* pneumonia. Microbiol Immunol 56:107–116. https://doi.org/10.1111/j.1348-0421.2011.00402.x.
25. Joly-Guillou ML, Wolff M, Pocidalo JJ, Walker F, Carbon C. 1997. Use of a new mouse model of *Acinetobacter baumannii* pneumonia to evaluate the postantibiotic effect of imipenem. Antimicrob Agents Chemother 41:345–351. https://doi.org/10.1128/AAC.41.2.345.
26. Lin L, Tan B, Pantapalangkoor P, Ho T, Baquir B, Tomaras A, Montgomery JI, Reilly U, Barbacci EG, Hujer K, Bonomo RA, Fernandez L, Hancock RE, Adams MD, French SW, Buslon VS, Spellberg B. 2012. Inhibition of LpxC protects mice from resistant *Acinetobacter baumannii* by modulating inflammation and enhancing phagocytosis. mBio 3:e00312-12. https://doi.org/10.1128/mBio.00312-12.
27. Bruhn KW, Dekitani K, Nielsen TB, Pantapalangkoor P, Spellberg B. 2016. Ly6G-mediated depletion of neutrophils is dependent on macrophages. Results Immunol 6:5–7. https://doi.org/10.1016/j.rinim.2015.12.001.
28. Zec K, Volke J, Vijitha N, Thiebes S, Gunzer M, Kurts C, Engel DR. 2016. Neutrophil migration into the infected uroepithelium is regulated by the crosstalk between resident and helper macrophages. Pathogens 5:15. https://doi.org/10.3390/pathogens5010015.
29. Mantovani A, Cassatella MA, Costantini C, Jaillon S. 2011. Neutrophils in the activation and regulation of innate and adaptive immunity. Nat Rev Immunol 11:519–531. https://doi.org/10.1038/nri3024.
30. Mittal M, Siddiqui MR, Tran K, Reddy SP, Malik AB. 2014. Reactive oxygen species in inflammation and tissue injury. Antioxid Redox Signal 20:1126–1167. https://doi.org/10.1089/ars.2012.5149.
31. Green ER, Juttukonda LJ, Skaar EP. 2020. The manganese-responsive transcriptional regulator MumR protects *Acinetobacter baumannii* from oxidative stress. Infect Immun 88:e00762-19. https://doi.org/10.1128/IAI.00762-19.
32. Juttukonda LJ, Green ER, Lonergan ZR, Heffern MC, Chang CJ, Skaar EP. 2018. *Acinetobacter baumannii* OxyR regulates the transcriptional response to hydrogen peroxide. Infect Immun 87:e00413-18. https://doi.org/10.1128/IAI.00413-18.
33. Lagasse E, Weissman IL. 1994. bcl-2 inhibits apoptosis of neutrophils but not their engulfment by macrophages. J Exp Med 179:1047–1052. https://doi.org/10.1084/jem.179.3.1047.
34. Savill JS, Wyllie AH, Henson JE, Walport MJ, Henson PM, Haslett C. 1989. Macrophage phagocytosis of aging neutrophils in inflammation. Programmed cell death in the neutrophil leads to its recognition by macrophages. J Clin Invest 83:865–875. https://doi.org/10.1172/JCI113970.
35. Cox G, Crossley J, Xing Z. 1995. Macrophage engulfment of apoptotic neutrophils contributes to the resolution of acute pulmonary inflammation *in vivo*. Am J Respir Cell Mol Biol 12:232–237. https://doi.org/10.1165/ajrcmb.12.2.7865221.
36. Huynh ML, Fadok VA, Henson PM. 2002. Phosphatidylserine-dependent ingestion of apoptotic cells promotes TGF-beta1 secretion and the resolution of inflammation. J Clin Invest 109:41–50. https://doi.org/10.1172/JCI11638.
37. Savill J, Dransfield I, Gregory C, Haslett C. 2002. A blast from the past: clearance of apoptotic cells regulates immune responses. Nat Rev Immunol 2:965–975. https://doi.org/10.1038/nri957.
38. Kamoshida G, Tansho-Nagakawa S, Kikuchi-Ueda T, Nakano R, Hikosaka K, Nishida S, Ubagai T, Higashi S, Ono Y. 2016. A novel bacterial transport mechanism of *Acinetobacter baumannii* via activated human neutrophils through interleukin-8. J Leukoc Biol 100:1405–1412. https://doi.org/10.1189/jlb.4AB0116-023RR.
39. Inglis TJ, Lim TM, Ng ML, Tang EK, Hui KP. 1995. Structural features of tracheal tube biofilm formed during prolonged mechanical ventilation. Chest 108:1049–1052. https://doi.org/10.1378/chest.108.4.1049.
40. Rossi E, Longo F, Barbagallo M, Peano C, Consolandi C, Pietrelli A, Jaillon S, Garlanda C, Landini P. 2016. Glucose availability enhances lipopolysaccharide production and immunogenicity in the opportunistic pathogen *Acinetobacter baumannii*. Future Microbiol 11:335–349. https://doi.org/10.2217/fmb.15.153.
41. Erridge C, Moncayo-Nieto OL, Morgan R, Young M, Poxton IR. 2007. *Acinetobacter baumannii* lipopolysaccharides are potent stimulators of human monocyte activation via Toll-like receptor 4 signalling. J Med Microbiol 56:165–171. https://doi.org/10.1099/jmm.0.46823-0.
42. Ubagai T, Nakano R, Nakano A, Kamoshida G, Ono Y. 2015. Gene expression analysis in human polymorphonuclear leukocytes stimulated by LPSs from nosocomial opportunistic pathogens. Innate Immun 21:802–812. https://doi.org/10.1177/1753425915605892.
43. Abdulkareem AF, Lee HH, Ahmadi M, Martinez LR. 2015. Fungal serotype-specific differences in bacterial-yeast interactions. Virulence 6:652–657. https://doi.org/10.1080/21505594.2015.1066962.
44. Hahn HP. 1997. The type-4 pilus is the major virulence-associated adhesin of *Pseudomonas aeruginosa*–a review. Gene 192:99–108. https://doi.org/10.1016/s0378-1119(97)00116-9.
45. Barbosa FM, Fonseca FL, Holandino C, Alviano CS, Nimrichter L, Rodrigues ML. 2006. Glucuronoxylomannan-mediated interaction of *Cryptococcus neoformans* with human alveolar cells results in fungal internalization and host cell damage. Microbes Infect 8:493–502. https://doi.org/10.1016/j.micinf.2005.07.027.

46. Patel D, Desai GM, Frases S, Cordero RJ, DeLeon-Rodriguez CM, Eugenin EA, Nosanchuk JD, Martinez LR. 2013. Methamphetamine enhances *Cryptococcus neoformans* pulmonary infection and dissemination to the brain. mBio 4:e00400-13. https://doi.org/10.1128/mBio.00400-13.
47. Matute-Bello G, Acute Lung Injury in Animals Study Group, Downey G, Moore BB, Groshong SD, Matthay MA, Slutsky AS, Kuebler WM. 2011. An official American Thoracic Society workshop report: features and measurements of experimental acute lung injury in animals. Am J Respir Cell Mol Biol 44:725–738. https://doi.org/10.1165/rcmb.2009-0210ST.
48. Rozentsvit A, Vinokur K, Samuel S, Li Y, Gerdes AM, Carrillo-Sepulveda MA. 2017. Ellagic acid reduces high glucose-induced vascular oxidative stress through ERK1/2/NOX4 signaling pathway. Cell Physiol Biochem 44:1174–1187. https://doi.org/10.1159/000485448.
49. Swamydas M, Luo Y, Dorf ME, Lionakis MS. 2015. Isolation of mouse neutrophils. Curr Protoc Immunol 110:3.20.1–3.20.15. https://doi.org/10.1002/0471142735.im0320s110.
50. Zhang X, Goncalves R, Mosser DM. 2008. The isolation and characterization of murine macrophages. Curr Protoc Immunol 14:14.1. https://doi.org/10.1002/0471142735.im1401s83.
51. Strober W. 2001. Trypan blue exclusion test of cell viability. Curr Protoc Immunol 21:A.3B.1–A.3B.2. https://doi.org/10.1002/0471142735.ima03bs21.